

Published in final edited form as:

*J Mol Biol.* 2011 January 7; 405(1): 105–112. doi:10.1016/j.jmb.2010.10.010.

## Robust mechanosensing and tension generation by myosin VI

Peiyong Chuan<sup>1</sup>, James A. Spudich<sup>1</sup>, and Alexander R. Dunn<sup>2</sup>

<sup>1</sup>Dept. of Biochemistry, Stanford University School of Medicine, Stanford, CA 94305, USA

<sup>2</sup>Dept. of Chemical Engineering, Stanford University, Stanford, CA 94305, USA

### Abstract

Myosin VI is a molecular motor that is thought to function as both a transporter and a cytoskeletal anchor *in vivo*. Here we use optical tweezers to examine force generation by single molecules of myosin VI under physiological nucleotide concentrations. We find that myosin VI is an efficient transporter at loads up to ~2 pN but acts as a cytoskeletal anchor at higher loads. Our data and resulting model are consistent with an indirect coupling of global structural motions to nucleotide binding and release. The model provides a mechanism by which load may regulate the dual functions of myosin VI *in vivo*. Our results suggest that myosin VI kinetics are tuned such that the motor maintains a consistent level of mechanical tension within the cell, a property potentially shared by other mechanosensitive proteins.

### Keywords

single molecule biophysics; optical tweezers; molecular motors; mechanical force; cytoskeleton

### Introduction

Myosin VI uses energy from ATP hydrolysis to transport cargo along actin filaments, and is also thought to function as a cytoskeletal anchor. Myosin VI plays critical roles in important biological processes such as development<sup>1</sup>, cardiac function<sup>2</sup> and hearing<sup>3</sup>. Proposed biological roles for myosin VI include both vesicle transport and the structural maintenance of the golgi apparatus and inner-ear stereocilia (reviewed in ref. 4).

Many cellular structures, including stereocilia, likely exist under mechanical tension, both to maintain their shape and to better transduce mechanical signals<sup>5</sup>. Myosin VI is proposed to play a critical structural role in the inner-ear stereocilia by generating and maintaining tension at the base of the stereocilia membrane. Previous models, however, predict that modest loads (<1 pN) should cause myosin VI to essentially stop stepping at physiological ATP and ADP concentrations<sup>6</sup>. We sought to clarify whether (and how) myosin VI can function as both a cellular transporter and anchor, generating and maintaining force *in vivo*, and to better understand how its dual roles may be regulated in the cell.

---

© 2010 Elsevier Ltd. All rights reserved.

**Publisher's Disclaimer:** This is a PDF file of an unedited manuscript that has been accepted for publication. As a service to our customers we are providing this early version of the manuscript. The manuscript will undergo copyediting, typesetting, and review of the resulting proof before it is published in its final citable form. Please note that during the production process errors may be discovered which could affect the content, and all legal disclaimers that apply to the journal pertain.

## Results and Discussion

### Myosin VI is highly processive under physiological nucleotide conditions and low loads

We used a dual beam optical trap assay with force feedback<sup>6,7</sup> (Fig. 1a) to study the stepping kinetics of single myosin VI dimers under varying nucleotide concentrations and loads. Briefly, two polystyrene beads attached to ends of an actin filament are held in independently controlled optical traps. The actin filament is then allowed to interact with a surface-bound myosin VI molecule. Feedback control on one trap maintains the force applied on the myosin molecule as the motor walks along actin. Only forward steps were considered in our analysis.

The dependence of dwell time on ADP concentration in the presence of 1.5 mM ATP and various loads was first examined. Up to ~5  $\mu$ M ADP, the dwell time increased rapidly (stepping rate decreased) as the ADP concentration increased, in agreement with previous data<sup>6</sup> (Fig. 1b). Surprisingly, dwell times increased only *slowly* between 5  $\mu$ M ADP and 100  $\mu$ M ADP (Fig. 1c). The same biphasic behavior was observed under various loads, with higher loads being associated with longer dwell times (Figs. 1b, 1c). At physiologically relevant nucleotide concentrations<sup>8</sup> of 1.5 mM ATP and 100  $\mu$ M ADP, myosin VI was highly processive under loads of 0.5 pN, 1.0 pN (Fig. 1d) and 1.5 pN, stepping efficiently along the actin filament with average dwell times of 0.47 s, 0.69 s (Fig. 1e) and 1.05 s respectively.

### Force and ADP dependency of dwell times necessitate a new kinetic model for myosin VI

The hyperbolic dwell time vs. ADP concentration curves (Fig. 1c) strongly suggest a multi-step ADP binding process<sup>9,10</sup>, the simplest case of which is two-step ADP binding:  $AM \rightleftharpoons AM(D) \rightleftharpoons AMD$ . Here AM represents the myosin VI rear head bound to actin and D represents ADP. AM and the initial AM(D) complex are in rapid equilibrium. Thus, strong ADP binding at saturation is limited by the rate of conversion from AM(D) to AMD.

Two other key observations from our data are that the ADP concentration at half-saturation does not depend markedly on force (Fig. 1c), and that dwell times are exponentially dependent on applied load at physiological ATP and ADP concentrations (Figs. 1c, 3a). This suggests that force acts analogously to an allosteric inhibitor. Borrowing from classical descriptions of allosteric regulation<sup>11</sup>, we propose that myosin VI can exist in one of two states, AM and AM\*. Force alters the equilibrium between the two states, favoring the AM\* state.

At high ATP concentrations (2 mM) and no added ADP, increasing load had only a small effect on the dwell time (Fig. 1f, **black**). In contrast, a significant increase in dwell time with increasing force was observed with the addition of only 1  $\mu$ M ADP (in the presence of 1.5 mM ATP; Fig. 1f, **blue**). We observed also that the dwell time is insensitive to ATP concentrations above 1.5 mM, as the stepping kinetics are dominated by slow ADP release (data not shown). Together, these data allow us to infer that the load-favored AM\* state has a greater affinity for ADP compared to the AM state, explaining the increase in dwell time with increasing load in the presence of ADP.

At low ATP concentrations (0.1 mM) and no added ADP, dwell time is also enhanced by increasing load (Fig. 1f, **red**). This behavior suggests that the AM\* state has a lower affinity for ATP compared to the AM state. These observations are consistent with previously published data<sup>6</sup> in which the effective ATP binding rate decreases modestly with load at low ATP concentrations.

## Kinetic model for myosin VI under load

To summarize, our key observations are that: 1) The hyperbolic dwell time vs. [ADP] curve implies a multi-step ADP binding process<sup>9,10</sup>; 2) The ADP concentration at half-saturation does not depend markedly on force and 3) Dwell times are exponentially dependent on applied load at physiological ATP and ADP concentrations, suggesting allosteric regulation of two interconverting myosin states by force; 4) Dwell times increase with load at low ATP concentrations, suggesting a modest decrease in ATP affinity with load. Multiple different kinetic models incorporating the above points were assessed, and the model that best accounts for both our and previously published data<sup>6</sup> is shown in Fig. 2.

In our model (Fig. 2a), myosin VI can exist in two states, M and M\*. Load alters the *force-sensitive equilibrium*  $K_{AM}(F)$  between the two interconverting actomyosin states AM and AM\* that have different nucleotide affinities, as reflected in the affinity or dissociation constants for ADP and ATP –  $K_{ADP1}$ ,  $K_{ADP2}$ ,  $K_{ATP1}$  and  $K_{ATP2}$  (included in  $k_{+T2}'$ , see below). AM\* is favored by load such as that applied by an optical trap<sup>6,7,12</sup>. AM, on the other hand, is more accessible under low external load, such as in bulk kinetic assays<sup>9,10</sup> and gold nanoparticle tracking experiments<sup>13</sup>. We note that force-dependent branching mechanisms have been previously proposed for DNA gyrase and RNA polymerase<sup>14,15</sup>.

In our study, only forward steps of dimeric myosin VI molecules were considered. The two heads of a myosin VI dimer have differing kinetics in the absence of load – the front head has a slower ADP release rate that prevents it from detaching from actin before the rear head, contributing to its processivity<sup>13</sup>. However, in our study we can consider only the kinetics of the *trailing* head since its release from actin determines the dwell time for forward steps. Backward steps, which were excluded from our analysis except at 3 pN load, are rare (2.1% on average, see Supplemental Information) and the frequency of backwards stepping is independent of load and ADP concentration up to ~ 2 pN.

Several simplifying assumptions were used in the model. First, our data confirm that ADP release from the rear head is load-independent (data not shown), consistent with previous studies<sup>6</sup>, so  $k_{-D1} = k_{-D2} = 4 \text{ s}^{-1}$ . Second, ATP binding to actomyosin VI results in immediate detachment from the actin filament and is essentially irreversible<sup>9</sup> such that  $k_{-T1} = k_{-T2} \approx 0$ . Third, we express ATP binding to AM\* as a 2<sup>nd</sup>-order rate constant  $k_{+T2}' = k_{+T2} / K_{ATP2}$  as our experimental conditions do not allow us to determine individually the affinity constant of AM\* for ATP,  $K_{ATP2}$ , and the rate of conversion from AM(T) → AMT,  $k_{+T2}$ . Lastly, we define the force-sensitive equilibrium constant  $K_{AM}$  as in Equation 1.  $K_{AM(0)}$  is the equilibrium constant at force  $F = 0$ , a positive  $F$  is a resistive load, and  $D$  is the sum of distances to the transition state from AM and AM\*<sup>16</sup>:

$$K_{AM} = K_{AM(0)} \exp\left(-\frac{FD}{k_b T}\right) \quad (\text{Eq. 1})$$

We determined parameters for our model using a global, weighted least-squares regression to the measured mean dwell times (Fig. 1b, 1c, 1f **solid curves**, Fig. 2b)<sup>9,17</sup>. Additional analyses of confidence contours<sup>18</sup> confirmed that the fit parameters are well-constrained. (Refer to Supplemental Information for details of regression analysis.)

### Load favors a distinct high ADP affinity AM\* state

The negative  $D$  value obtained from our model implies that the AM\* state is favored as load is increased. One possible physical interpretation of this is that backward load rotates the lever arm of post-stroke rigor myosin VI in the pre-stroke direction, resembling the ADP-bound state. The distance between the AM and AM\* energy wells in the model is  $D \approx 6.7$

nm. This value is consistent with a displacement of ~6 nm that would result from a 20° rotation of a 16 nm lever arm<sup>19</sup>, which has been shown to occur upon ADP binding<sup>20</sup>.

From the regression parameters, we observe that compared to AM, the load-favored AM\* experiences ~120× accelerated ADP binding ( $k_{+D2} / K_{ADP2} = 20 \mu\text{M}^{-1} \text{s}^{-1}$ ;  $k^{+D1} / K_{ADP1} = 0.17 \mu\text{M}^{-1} \text{s}^{-1}$ ) and ~5× slower ATP binding ( $k_{+T2}' = k_{+T2} / K_{ATP2} = 0.006 \mu\text{M}^{-1} \text{s}^{-1}$ ;  $k_{+T1} / K_{ATP1} = 0.031 \mu\text{M}^{-1} \text{s}^{-1}$ ). This is in qualitative agreement with a smaller acceleration in ADP binding observed with single-headed myosin VI under load<sup>21</sup>; the difference in magnitude may result from differences in dimerization state, lever arm length, or load application geometry. With 1.5 mM ATP and load, the initial dramatic rise in dwell time at low ADP concentrations (Fig. 1b) is dominated by the effective competition of ADP with ATP for binding to the higher ADP affinity AM\* state. At greater ADP concentrations (> ~5 μM), ADP binding to AM\* saturates (Fig. 1c), and additional ADP mainly binds to the relatively ADP-insensitive AM state. This allows the stepping kinetics of myosin VI to remain relatively constant over a wide range of ADP concentrations, ensuring that the motor functions consistently regardless of fluctuations in cellular nucleotide concentrations.

We note that the apparent ADP affinity of 0.18 μM for AM\* is tight for a single-step binding reaction. Even with a diffusion-limited on-rate constant, the off-rate constant would be ~18 s<sup>-1</sup>, which is slow enough to influence the kinetics of ADP release. Since ADP release rate is independent of load, the AM\*(D) state is unlikely to correspond to a literal collision complex, and likely forms in a process with at least two elementary steps that we do not resolve.

### An independent conformational change is likely coupled to the lever arm swing and ADP binding

Models with two interconverting AM states have been proposed for several myosin I and II isoforms<sup>22–24</sup>. In these models, however, one form of AM is unable to bind nucleotide. Assuming that the equilibrium constant for interconversion of the two AM states is force-sensitive, this class of models proved to be inconsistent with our data as it does not predict the saturation of dwell time at low ADP concentrations that we observe.

Models in which AM(D) and AM\*(D) equilibrate also do not fit our data. Non-converting, or slowly converting AM(D) and AM\*(D) states are necessary to explain both the initial rapid rise in dwell time observed with a few micromolar ADP, *and* the very modest increase in dwell time with increased [ADP] between 10 and 100 μM. We note that our model is consistent with prior bulk kinetic data used to support a model in which ADP binds to actomyosin VI to form two non-interconverting populations<sup>10</sup>.

A possible explanation for the bifurcating kinetic scheme is that AM and AM\* have differing affinities for Mg<sup>2+</sup>. [Mg<sup>2+</sup>] modulates the rate of ADP release from myosin VI (unpublished results). Bulk kinetics measurements with myosin V likewise indicate distinct binding and release kinetics for free ADP and Mg·ADP<sup>25,26</sup>. Other mechanisms could include coupling of the lever arm to conformational changes of the 50 kDa cleft, or movement of the P loop, which has been observed by crystallography to occur in myosin V upon ADP binding<sup>27</sup>.

We are unable to determine if AMD and AM\*D interconvert directly as the ADP off rates for both are very similar. However, if they are in rapid equilibrium, we can infer from the thermodynamic box that the equilibrium constant at F = 0 would be 120, with the same value of D = -6.7 nm. This means that at equilibrium, the molecules mostly populate the AM\*D rather than the AMD state, even at zero load, consistent with EM images<sup>20</sup>.

## Myosin VI exhibits long dwells under physiological nucleotide conditions and high loads

The model correctly predicts dwell times of myosin VI under physiological ATP and ADP conditions at forces of  $\geq 1.7$  pN (Fig. 3, red data points). At loads beyond the stall force of  $\sim 2$  pN, stepping kinetics increasingly reflect processes distinct from those included in our model. With 2 mM ATP and in the absence of ADP, we observe a “stalling” behavior characterized by a rapid rise in dwell time of forward steps at forces beyond  $\sim 2$  pN (data not shown), consistent with previous work<sup>6</sup>. Our model does not incorporate a parameter to account for this behavior, which we believe results when applied load physically prevents the detached head from reattaching to the filament in the lead position.

At 3 pN backward load, myosin VI exhibits long dwells (Fig. 3, mean =  $8.8 \pm 1.1$  s), and takes up to four backsteps before releasing from actin (Supplemental Information). Previous work shows that the unbinding force of a single ADP-bound myosin VI head under rearward force is  $2.6 \pm 0.1$  pN<sup>21</sup>. At 3 pN the backward steps we observe are thus likely to result from detachment of the ADP-bound front head. We infer that rear head detachment is as slow as or slower than front head detachment, as evidenced by the predominance of backsteps.

We emphasize that this backstepping behavior is distinct from the forward stepping in our earlier analyses. However, while we cannot rule out a coincidence, the agreement of dwell times measured at super-stall forces with our model supports the likelihood that rear head detachment is at least comparably slower than the rate of front head detachment under these conditions. Regardless of the specific mechanism, slow backward stepping and detachment additionally provide an appealing mechanism for the gradual release of excess mechanical tension *in vivo*.

## Our data and model suggest that lever arm motions are indirectly coupled to changes within the active site

The effect of applied load on myosins I<sup>28</sup>, V<sup>21,29,30</sup>, and VI<sup>6,21</sup>, and kinesin<sup>31</sup> has been described using rate constants that are directly altered by load. For myosin VI, previous work<sup>6</sup> proposed that load directly increases the ADP binding rate constant  $k_{-1}$  (Equation 2), which corresponds to  $k_{+D1}/K_{ADP1}$  in Fig. 2:

$$k_{-1} = k_{(0)} \exp\left(-\frac{F\delta}{k_b T}\right) \quad (\text{Eq. 2})$$

Although this model fit the data available at the time, it predicts a strong dependence of dwell time on ADP concentration, and that modest loads ( $< 1$  pN) should cause myosin VI to essentially stop stepping at physiological ATP and ADP concentrations. Instead, we observe that myosin VI is highly processive and its stepping rates at a given load remain relatively constant over a wide range of physiologically relevant ADP concentrations (Fig. 1c, 1d). A force-sensitive conformational equilibrium accounts for our data: the rapid increase in dwell times at low [ADP] reflects ADP binding by AM\*, while the subsequent plateau reflects lower-affinity ADP binding to AM. The differences in nucleotide affinity may be related to allosteric effects of load application on the nucleotide pocket, resulting in conformation changes that block ATP binding but stabilize ADP.

Equation 2 corresponds to a picture of enzymatic catalysis where motion within the enzyme occurs simultaneously with chemical changes in the active site<sup>32,33</sup>. This view provides an intuitive description of molecular motors: for instance, ATP hydrolysis and phosphate release are proposed to drive global structural transformations in myosin<sup>34</sup>. However, recent studies suggest an alternative view in which global conformational dynamics are more loosely coupled to reactions within the active site: NMR experiments suggest that protein

conformational changes may precede and even limit the rate of the subsequent chemical reactions<sup>35–37</sup>. Single-molecule fluorescence experiments on cholesterol oxidase<sup>38</sup>,  $\beta$ -galactosidase<sup>39</sup>, and lipase<sup>40</sup> likewise imply that enzymes interconvert between distinct conformations with different catalytic abilities.

Our model represents a case where a global conformational change (shift from the AM state to the AM\* state) controls chemical changes at the active site (nucleotide binding). Our results are thus consistent with models of catalysis in which enzymatic structural motions can precede, and limit, the rate of the corresponding catalytic step. We note that ensemble myosin kinetics likewise suggest that structural isomerization steps precede nucleotide binding<sup>22,41</sup>. Probing the kinetics of myosin VI under load has allowed us to distinguish the probable mechanism that couples global conformational dynamics to changes in the active site. Determining whether other mechanoenzymes also display similar indirect coupling of catalysis and motion remains an exciting challenge for the future.

### Biological significance

Our model provides a simple mechanism to explain how the dual functions of myosin VI may be regulated *in vivo*. At low loads, myosin VI could function as an efficient transporter while taking 2–3 steps  $s^{-1}$  (Fig. 3, left), slowing down with increasing loads up to ~2 pN (Fig. 3, center). At forces greater than ~2.5 pN, myosin VI converts to a dynamic anchor, taking slow backsteps before detaching from actin. In this way, myosin VI is able to maintain tension at ~2 pN and relieve forces greater than ~2.5 pN. Such dual load-dependent functions are likely to have significance *in vivo*, for instance in the inner-ear hair cells where myosin VI is proposed to *transport* cargo within the stereocilia as well as to *anchor* the apical cell membrane to the base of the stereocilia<sup>3</sup>, maintaining their structural integrity. We speculate that other mechanosensitive motors may employ conceptually similar chemomechanical mechanisms to maintain the delicate balance of forces within living cells.

## Materials and Methods

### Constructs and Protein Purification

Dimeric myosin VI construct was made using porcine myosin VI cDNA truncated at Arg<sup>992</sup> followed by a GCN4 leucine zipper, eYFP and a C-terminal Flag tag (DYKDDDDK) for purification. Cloning, protein expression and purification were performed as previously described<sup>13</sup>.

### Optical Trapping

Single molecule optical trapping assays with force feedback were performed as previously described<sup>6</sup>. Optical trap data was collected using LabVIEW (National Instruments) and tabulated using algorithms developed in Matlab (Mathworks). Step positions were determined using a method developed closely based on a previous stepfinding algorithm<sup>42</sup>. Errors for dwell times were obtained by bootstrapping with 1000 replicates to get the standard error of the mean (SEM).

### Nucleotide Purification

Because ATP stocks can contain 1% or more ADP contamination, ATP that was used in assays without an ATP-regeneration system was purified by liquid chromatography. An ÄKTA FPLC system (GE Healthcare) was used with an anion-exchange column (MonoQ HR 5/5, GE Healthcare). Nucleotide was loaded on the column with 25 mM imidazole HCl, 4 mM MgCl<sub>2</sub> (pH 7). The elution buffer used was 25 mM imidazole HCl, 4 mM MgCl<sub>2</sub>, 500 mM KCl (pH 7). 13% elution buffer was flowed over the column until AMP was eluted, and



ATP was subsequently eluted with a 13%–55% gradient of elution buffer. ADP was purified identically.

### Data Analysis

Refer to Supplemental Information for details on kinetic modeling and regression analysis. Briefly, a global, weighted least-squares regression of the analytical solution for dwell time was performed on the data using Matlab, and verified in Prism (GraphPad Software, Inc.). Errors on the parameters were obtained by performing a parametric bootstrap with 2000 replicates. Confidence contour analyses based closely on algorithms previously described<sup>18</sup> were performed in Matlab to determine if the parameters are well constrained.

### Supplementary Material

Refer to Web version on PubMed Central for supplementary material.

### Acknowledgments

We thank David Altman, Jongmin Sung, Zev Bryant, Sivaraj Sivaramakrishnan and Mary Elting for helpful discussions. P.C. is an A\*STAR NSS(PhD) Scholar. A.R.D. is supported by a Burroughs Wellcome CASI. J.A.S. is supported by grant GM33289 from the NIH.

### References

1. Lin HP, Chen HM, Wei SY, Chen LY, Chang LH, Sun YJ, et al. Cell adhesion molecule Echinoid associates with unconventional myosin VI/Jaguar motor to regulate cell morphology during dorsal closure in *Drosophila*. *Dev Biol*. 2007; 311:423–433. [PubMed: 17936269]
2. Mohiddin SA, Ahmed ZM, Griffith AJ, Tripodi D, Friedman TB, Fananapazir L, et al. Novel association of hypertrophic cardiomyopathy, sensorineural deafness, and a mutation in unconventional myosin VI (MYO6). *J Med Genet*. 2004; 41:309–314. [PubMed: 15060111]
3. Hertzano R, Shalit E, Rzadzinska AK, Dror AA, Song L, Ron U, et al. A Myo6 mutation destroys coordination between the myosin heads, revealing new functions of myosin VI in the stereocilia of mammalian inner ear hair cells. *PLoS Genet*. 2008; 4 e1000207.
4. Buss F, Kendrick-Jones J. How are the cellular functions of myosin VI regulated within the cell? *Biochem Biophys Res Commun*. 2008; 369:165–175. [PubMed: 18068125]
5. Cai Y, Sheetz MP. Force propagation across cells: mechanical coherence of dynamic cytoskeletons. *Curr Opin Cell Biol*. 2009; 21:47–50. [PubMed: 19208463]
6. Altman D, Sweeney HL, Spudich JA. The mechanism of myosin VI translocation and its load-induced anchoring. *Cell*. 2004; 116:737–749. [PubMed: 15006355]
7. Rock RS, Ramamurthy B, Dunn AR, Beccafico S, Rami BR, Morris C, et al. A flexible domain is essential for the large step size and processivity of myosin VI. *Mol Cell*. 2005; 17:603–609. [PubMed: 15721263]
8. Stryer, L. *Biochemistry*. 4th edn. New York: W.H. Freeman & Company; 1995.
9. Robblee JP, Olivares AO, de la Cruz EM. Mechanism of nucleotide binding to actomyosin VI: evidence for allosteric head-head communication. *J Biol Chem*. 2004; 279:38608–38617. [PubMed: 15247304]
10. Sweeney HL, Park H, Zong AB, Yang Z, Selvin PR, Rosenfeld SS. How myosin VI coordinates its heads during processive movement. *EMBO J*. 2007; 26:2682–2692. [PubMed: 17510632]
11. Fersht, A. *Structure and Mechanism in Protein Science: A Guide to Enzyme Catalysis and Protein Folding*. New York; 1999.
12. Rock RS, Rice SE, Wells AL, Purcell TJ, Spudich JA, Sweeney HL. Myosin VI is a processive motor with a large step size. *Proc Natl Acad Sci U S A*. 2001; 98:13655–13659. [PubMed: 11707568]

13. Dunn AR, Chuan P, Bryant Z, Spudich JA. Contribution of the myosin VI tail domain to processive stepping and intramolecular tension sensing. *Proc Natl Acad Sci U S A*. 2010; 107:7746–7750. [PubMed: 20385849]
14. Abbondanzieri EA, Greenleaf WJ, Shaevitz JW, Landick R, Block SM. Direct observation of base-pair stepping by RNA polymerase. *Nature*. 2005; 438:460–465. [PubMed: 16284617]
15. Nollmann M, Stone MD, Bryant Z, Gore J, Crisona NJ, Hong SC, et al. Multiple modes of *Escherichia coli* DNA gyrase activity revealed by force and torque. *Nat Struct Mol Biol*. 2007; 14:264–271. [PubMed: 17334374]
16. Wang MD, Schnitzer MJ, Yin H, Landick R, Gelles J, Block SM. Force and velocity measured for single molecules of RNA polymerase. *Science*. 1998; 282:902–907. [PubMed: 9794753]
17. Efron, B.; Tibshirani, R. An introduction to the bootstrap. New York: Chapman & Hall; 1993.
18. Johnson KA, Simpson ZB, Blom T. FitSpace explorer: an algorithm to evaluate multidimensional parameter space in fitting kinetic data. *Anal Biochem*. 2009; 387:30–41. [PubMed: 19168024]
19. Spink BJ, Sivaramakrishnan S, Lipfert J, Doniach S, Spudich JA. Long single alpha-helical tail domains bridge the gap between structure and function of myosin VI. *Nat Struct Mol Biol*. 2008; 15:591–597. [PubMed: 18511944]
20. Wells AL, Lin AW, Chen LQ, Safer D, Cain SM, Hasson T, et al. Myosin VI is an actin-based motor that moves backwards. *Nature*. 1999; 401:505–508. [PubMed: 10519557]
21. Oguchi Y, Mikhailenko SV, Ohki T, Olivares AO, De La Cruz EM, Ishiwata S. Load-dependent ADP binding to myosins V and VI: implications for subunit coordination and function. *Proc Natl Acad Sci U S A*. 2008; 105:7714–7719. [PubMed: 18509050]
22. Geeves MA, Perreault-Micale C, Coluccio LM. Kinetic analyses of a truncated mammalian myosin I suggest a novel isomerization event preceding nucleotide binding. *J Biol Chem*. 2000; 275:21624–21630. [PubMed: 10781577]
23. Lewis JH, Lin T, Hokanson DE, Ostap EM. Temperature dependence of nucleotide association and kinetic characterization of myo1b. *Biochemistry*. 2006; 45:11589–11597. [PubMed: 16981718]
24. Bloemink MJ, Adamek N, Reggiani C, Geeves MA. Kinetic analysis of the slow skeletal myosin MHC-I isoform from bovine masseter muscle. *J Mol Biol*. 2007; 373:1184–1197. [PubMed: 17900618]
25. Rosenfeld SS, Houdusse A, Sweeney HL. Magnesium regulates ADP dissociation from myosin V. *J Biol Chem*. 2005; 280:6072–6079. [PubMed: 15579901]
26. Hannemann DE, Cao W, Olivares AO, Robblee JP, De La Cruz EM. Magnesium, ADP, and actin binding linkage of myosin V: evidence for multiple myosin V-ADP and actomyosin V-ADP states. *Biochemistry*. 2005; 44:8826–8840. [PubMed: 15952789]
27. Coureux PD, Sweeney HL, Houdusse A. Three myosin V structures delineate essential features of chemo-mechanical transduction. *EMBO J*. 2004; 23:4527–4537. [PubMed: 15510214]
28. Laakso JM, Lewis JH, Shuman H, Ostap EM. Myosin I can act as a molecular force sensor. *Science*. 2008; 321:133–136. [PubMed: 18599791]
29. Veigel C, Schmitz S, Wang F, Sellers JR. Load-dependent kinetics of myosin-V can explain its high processivity. *Nat Cell Biol*. 2005; 7:861–869. [PubMed: 16100513]
30. Clemen AE, Vilfan M, Jaud J, Zhang J, Barmann M, Rief M. Force-dependent stepping kinetics of myosin-V. *Biophys J*. 2005; 88:4402–4410. [PubMed: 15764664]
31. Block SM, Asbury CL, Shaevitz JW, Lang MJ. Probing the kinesin reaction cycle with a 2D optical force clamp. *Proc Natl Acad Sci U S A*. 2003; 100:2351–2356. [PubMed: 12591957]
32. Koshland DE. Application of a Theory of Enzyme Specificity to Protein Synthesis. *Proc Natl Acad Sci U S A*. 1958; 44:98–104. [PubMed: 16590179]
33. Koshland DE Jr, Nemethy G, Filmer D. Comparison of experimental binding data and theoretical models in proteins containing subunits. *Biochemistry*. 1966; 5:365–385. [PubMed: 5938952]
34. Spudich JA. The myosin swinging cross-bridge model. *Nat Rev Mol Cell Biol*. 2001; 2:387–392. [PubMed: 11331913]
35. Boehr DD, McElheny D, Dyson HJ, Wright PE. The dynamic energy landscape of dihydrofolate reductase catalysis. *Science*. 2006; 313:1638–1642. [PubMed: 16973882]



36. Eisenmesser EZ, Millet O, Labeikovsky W, Korzhnev DM, Wolf-Watz M, Bosco DA, et al. Intrinsic dynamics of an enzyme underlies catalysis. *Nature*. 2005; 438:117–121. [PubMed: 16267559]
37. Cole R, Loria JP. Evidence for flexibility in the function of ribonuclease A. *Biochemistry*. 2002; 41:6072–6081. [PubMed: 11994002]
38. Lu HP, Xun L, Xie XS. Single-molecule enzymatic dynamics. *Science*. 1998; 282:1877–1882. [PubMed: 9836635]
39. English BP, Min W, van Oijen AM, Lee KT, Luo G, Sun H, et al. Ever-fluctuating single enzyme molecules: Michaelis-Menten equation revisited. *Nat Chem Biol*. 2006; 2:87–94. [PubMed: 16415859]
40. Flomenbom O, Velonia K, Loos D, Masuo S, Cotlet M, Engelborghs Y, et al. Stretched exponential decay and correlations in the catalytic activity of fluctuating single lipase molecules. *Proc Natl Acad Sci U S A*. 2005; 102:2368–2372. [PubMed: 15695587]
41. Robblee JP, Cao W, Henn A, Hannemann DE, De La Cruz EM. Thermodynamics of nucleotide binding to actomyosin V and VI: a positive heat capacity change accompanies strong ADP binding. *Biochemistry*. 2005; 44:10238–10249. [PubMed: 16042401]
42. Kerssemakers JW, Munteanu EL, Laan L, Noetzel TL, Janson ME, Dogterom M. Assembly dynamics of microtubules at molecular resolution. *Nature*. 2006; 442:709–712. [PubMed: 16799566]

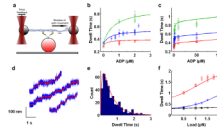
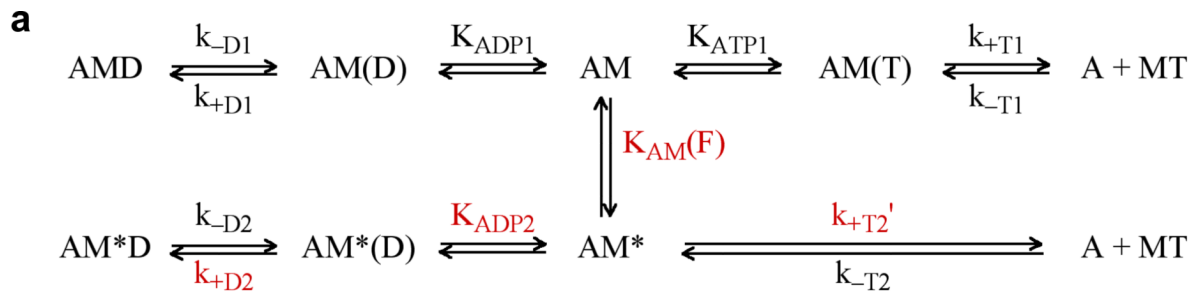


**Figure 1. Optical trapping data and regression curves from kinetic model**

**a)** Optical trapping assay. Two polystyrene beads attached to ends of an actin filament are held in independently controlled optical traps. The actin filament is brought into contact with a surface platform bead-bound myosin VI molecule. Feedback control on one trap maintains the force applied on the myosin molecule as the motor walks along actin. **b,c)** Dependence of dwell time on **b)** low ADP concentrations up to  $2.5 \mu\text{M}$ ; **c)** ADP concentrations up to  $100 \mu\text{M}$ , in the presence of  $2 \text{ mM}$  ATP (for zero ADP only) or  $1.5 \text{ mM}$  ATP and  $0.5 \text{ pN}$  (*red*),  $1.0 \text{ pN}$  (*blue*) and  $1.5 \text{ pN}$  (*green*) load. Within each condition, each data point represents a different myosin VI molecule. *Squares* are our measured dwell times, *asterisks* are data from ref. 6. Errors for dwell times were obtained by bootstrapping with 1000 replicates to get the standard error of the mean (SEM). **d)** Stepping traces of myosin VI in the optical trap in the presence of  $1.5 \text{ mM}$  ATP,  $100 \mu\text{M}$  ADP and  $1 \text{ pN}$  load. Filtered bead positions (*red traces*) are overlaid on raw bead positions (*blue traces*). **e)** Dwell time histogram for one molecule under the same conditions as in **d)**. Average dwell time is  $0.69 \pm 0.03 \text{ s}$ . *Red curve* is the predicted dwell time distribution based on our model. **f)** Dependence of dwell time on load in the presence of  $2 \text{ mM}$  ATP (*black*),  $1.5 \text{ mM}$  ATP plus  $1 \mu\text{M}$  ADP (*blue*), and  $0.1 \text{ mM}$  ATP (*red*). **b,c,f)** Best fit curves to dwell time data from global weighted least squares regression (*solid lines*). Refer to Supplemental Information for details of data analysis.



**b**

	$k_{-D1} = k_{-D2}$ (s <sup>-1</sup> )	$k_{+D1}$ (s <sup>-1</sup> )	$K_{\text{ADP1}}$ (μM)	$K_{\text{ATP1}}$ (μM)	$k_{+T1}$ (s <sup>-1</sup> )	$K_{\text{ADP2}}$ (μM)	$k_{+D2}$ (s <sup>-1</sup> )	$k_{+T2'}$ (μM <sup>-1</sup> s <sup>-1</sup> )	$K_{\text{AM}(0)}$	$D$ (nm)
Value	4.0	366	2200	5600	176	0.18	3.6	$5.6 \times 10^{-3}$	1.0	-6.7
Error						0.03	0.8	$0.3 \times 10^{-3}$	0.1	0.2

**Figure 2. Kinetic model and parameters for myosin VI under load**

**a)** Kinetic scheme for myosin VI under load. Myosin exists in two states, M and M\*. AM represents the myosin VI rear head (M) bound to actin (A), and D and T represent ADP and ATP respectively.  $K_{\text{AM(F)}} = K_{\text{AM}(0)} \exp(-FD/k_{\text{B}}T)$  is the force-sensitive equilibrium constant between AM and AM\*. All other uppercase K's are affinity constants, and lowercase k's are rate constants. **b)** Previously determined parameters<sup>6,9</sup> that were fixed in the regression are in *black*. Values from the regression and their errors are in *red*. Each data point was weighted by the inverse of its squared standard error of the mean. Errors on the parameters were determined by assuming that each data point follows a normal distribution centered at the mean with a standard deviation of SEM, and performing a parametric bootstrap<sup>17</sup> with 2000 replicates. Refer to Supplemental Information for details of regression analysis.

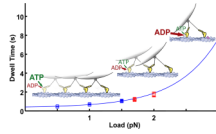


**Figure 3. The dual functions of myosin VI are regulated by load *in vivo***

**a)** Dependence of dwell time on load under physiological 1.5 mM ATP and 100  $\mu$ M ADP (data used in regression: *blue points*; model: *blue curve*). The model correctly predicts dwell times at higher forces (*red*). Within each condition, each data point represents a different myosin VI molecule. Cartoons depict myosin VI motors stepping along actin while attached via adapter proteins (*grey ovals*) to a membrane. At low loads, the rate of ADP binding (*red arrow*) is low (leftmost cartoon). The rear head predominantly binds ATP (*green arrow*), resulting in 2–3 steps  $s^{-1}$ . At moderate forces ADP competes with ATP for binding to the rear head, slowing the motor to less than 1 step  $s^{-1}$  (center). At forces greater than  $\sim 2.5$  pN, the stepping rate decreases rapidly as ADP out-competes ATP for binding (right). The motor takes slow backsteps before detaching from actin (see Supplemental Information). In this way, M6 is able to maintain tension at  $\sim 2$  pN and relieve forces greater than  $\sim 2.5$  pN.